Nuclear-Reaction Studies with 65-MeV Alpha Particles on Zirconium*

C. R. BINGHAM,† M. L. HALBERT, AND R. H. BASSEL‡

Oak Ridge National Laboratory, Oak Ridge, Tennessee

(Received 23 March 1966)

Differential cross sections for elastic and inelastic scattering and $(\alpha,{}^3He)$ reactions were measured for 65-MeV alpha particles on ${}^{90}Zr$, ${}^{91}Zr$, and ${}^{92}Zr$. Excellent optical-model fits to the elastic data were obtained with four-parameter Woods-Saxon potentials having a real depth of about 35 MeV. A continuum of fits almost as good was found for a class of deeper wells. Distorted-wave predictions for all the inelastic groups studied were made with the collective model. The results were insensitive to the ambiguity in the potentials, and were quite successful for most of the groups. Where comparisons can be made, the values of the deformation parameter β_l are in agreement with results from Coulomb excitation and nuclear scattering of other particles. Exploratory calculations were made for single-particle excitation for the first 2^+ and 4^+ levels of ${}^{92}Zr$. The $(\alpha,{}^3He)$ cross sections were compared with zero-range distorted-wave predictions. Good fits to the angular distributions were obtained by selection among potentials which provide fits for elastic scattering in the entrance and exit channels. Normalization of the predictions to the data yielded spectroscopic factors in generally good agreement with results from (d,p) and (p,d) measurements for s and d states. In making this comparison, an empirical adjustment by a factor of 17.8 was included. The predictions for $g_{7/2}$ states were generally too small. Spin-orbit and nonlocal corrections do not improve the agreement. Some of the discrepancy may be due to the presence of small portions of the $h_{11/2}$ strength in the low-lying states.

I. INTRODUCTION

SINCE the introduction of the distorted-wave Born approximation, the inelastic scattering of alpha particles has been extensively analyzed in terms of collective rotations and vibrations.[1] This method of analysis has been very successful in describing excitations to the first 2^+ and 3^- states of even-even nuclei. It is quite reasonable that such a model should work well for nuclei with many particles outside of closed shells, where collective motion is easily obtained. But, for nuclei with only a few particles outside of closed shells, shell effects may also be important. The inclusion of shell effects in calculations for inelastic scattering of alpha particles[2,3] and protons[4,5] has recently been studied. The gross structure of the angular distributions predicted by the distorted-wave theory is determined by the distorted waves and the angular momentum transferred in the reaction.[1,3] Hence, the shell model and collective model, when treated in the distorted-wave theory, give very similar angular distributions, although there are small differences.

The primary motivation for this experiment was to determine how well the collective model and shell model predict inelastic scattering of 65-MeV alpha particles from nuclei near closed shells and to see if either model gives a more consistent picture. The zirconium isotopes were chosen because of their proximity to closed shells, the good separation of the low excited states, and the availability of targets of separated zirconium isotopes.

The elastic cross sections were subjected to considerable theoretical study, both for their own sake and because of their usefulness in determining the optical-model parameters needed for theoretical prediction of reaction cross sections.[6] Other measurements of scattering of 65-MeV alpha particles[7] are for lighter nuclei; the highest energy data previously available for alpha scattering by Zr were obtained at 43 MeV.[8] Collective-model calculations were performed for all the inelastic angular distributions. For comparison, shell-model calculations were performed for a few selected states.

The experimental apparatus made possible the simultaneous accumulation of ${}^3He$ spectra from $(\alpha,{}^3He)$ reactions. Alpha-particle stripping has not been previously reported at this high an energy. The usefulness of the $(\alpha,{}^3He)$ reaction as a tool for nuclear spectroscopy was investigated by comparison with results of (d,p) reactions at lower energy.[9] The zero-range approximation was used in the stripping calculations. The effect of including nonlocal potentials was studied by using the local energy approximation.

Results for ${}^{90}Zr$, ${}^{91}Zr$, and ${}^{92}Zr$ targets are presented

[1] R. H. Bassel, G. R. Satchler, R. M. Drisko, and E. Rost, Phys. Rev. **128**, 2693 (1962); E. Rost, *ibid.* **128**, 2708 (1962).

[2] E. Sanderson, Nucl. Phys. **35**, 557 (1962); E. Sanderson and N. S. Wall, Phys. Letters **2**, 173 (1962); N. S. Wall, Argonne National Laboratory Report No. ANL-6848, 1964 (unpublished), p. 108; H. O. Funsten, N. R. Roberson, and E. Rost, Phys. Rev. **134**, B117 (1964); N. K. Glendenning and M. Veneroni, Phys. Letters 14, 228 (1965).

[3] G. R. Satchler, J. L. Yntema, and H. W. Broek, Phys. Letters **12**, 55 (1964).

[4] W. S. Gray, R. A. Kenefick, J. J. Kraushaar, and G. R. Satchler, Phys. Rev. **142**, 735 (1966).

[5] M. B. Johnson, L. W. Owen, and G. R. Satchler, Phys. Rev. **142**, 748 (1966).

[6] L. L. Lee, J. P. Schiffer, B. Zeidman, G. R. Satchler, R. M. Drisko, and R. H. Bassel, Phys. Rev. **136**, B971 (1964).

[7] P. Darriulat, G. Igo, H. G. Pugh, J. M. Meriwether, and S. Yamabe, Phys. Rev. **134**, B42 (1964); B. G. Harvey, E. J. M. Rivet, A. Springer, J. M. Meriwether, W. B. Jones, J. H. Elliott, and P. Darriulat, Nucl. Phys. **52**, 465 (1964).

[8] H. W. Broek and J. L. Yntema, Phys. Rev. **138**, B334 (1965).

[9] B. L. Cohen and O. V. Chubinsky, Phys. Rev. **131**, 2184 (1963).

here. A more complete account may be found in Ref. 10. Analysis is now in progress on data obtained with alpha particles on ^{94}Zr and ^{96}Zr targets and with ^{3}He bombardments of ^{92}Zr.

II. EXPERIMENTAL METHOD

The Oak Ridge Isochronous Cyclotron (ORIC) accelerated the 65-MeV alpha particles used in this experiment. The ORIC is a fixed-frequency, variable-energy cyclotron with an azimuthally varying magnetic field.[11] The beam was analyzed by a 153° $n = \frac{1}{2}$ magnet with a 72-in. radius of curvature.

Most of the measurements were carried out in a 30-in. diameter scattering chamber. Because of the rapid oscillations in the scattering angluar distributions, it was desirable to obtain an angular resolution of less than 1° and to stabilize the beam position on the target. For these purposes the beam was collimated near the entrance of the scattering chamber. The beam spot on the target was about 0.070 in. wide and $\frac{1}{4}$ in. high. The detector aperture was 0.070 in. wide and about $\frac{3}{16}$ in. high, placed at a distance of about $8\frac{1}{2}$ in. from the center of the chamber. The detectors were mounted inside the chamber on a movable disc which could be remotely positioned to within 0.05°. The targets were located at the center of the chamber. Prior to the installation of the 153° magnet some data were taken in a 24 in. chamber with similar geometry.

The ^{90}Zr and ^{92}Zr targets were foils rolled by the Oak Ridge target preparation facility to a thickness of about 6 mg/cm². The ^{91}Zr target was made of three layers of foil, each rolled to a thickness of about 0.9 mg/cm². The target thicknesses were determined by measuring the energy loss of ^{241}Am alpha particles in passing through them. The foils were also scanned to check their uniformity and were found to be uniform within 10%. The beam made a black spot on the targets during bombardment. The thicknesses of the targets at these spots are the values given in Table I. In calculating these thicknesses, the energy loss of the alpha particles in Zr was estimated by interpolation in the tables given by Whaling.[12] The results were insensitive to the details of this procedure. The ^{90}Zr target was also weighed, and the results were in satisfactory agreement. In calculating the inelastic and ($\alpha,^{3}$He) cross sections, corrections were included for the isotopic abundances given in Table I.

The accuracy of the measured cross sections was limited mainly by the target thickness determinations, and is estimated to be about 10%. For the weakest transitions, however, counting statistics and back-
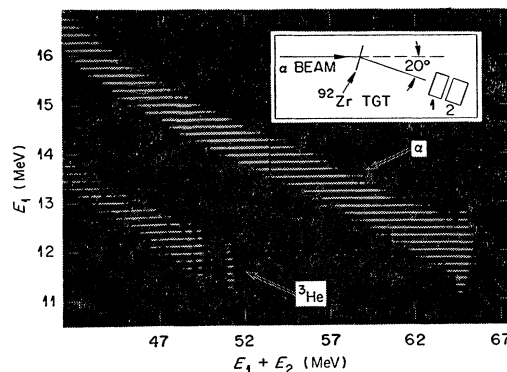
[10] C. R. Bingham, 1965, Oak Ridge National Laboratory Internal Report No. TM-1336, 1965 (unpublished).

[11] R. J. Jones, E. D. Hudson, R. S. Livingston, R. S. Lord, M. B. Marshall, W. R. Smith, W. H. White, Jr., and R. E. Worsham, Nucl. Instr. Methods **18**, 19, 46 (1962); Oak Ridge National Laboratory reports Nos. ORNL-3630 (1963) and ORNL-3800 (1964).

[12] W. Whaling, in *Handbuch der Physik*, edited by S. Flügge (Springer-Verlag, Berlin, 1958), Vol. 34, p. 193–217.

FIG. 1. Photograph of analyzer display. All channels containing at least one count are shown by a bright spot. The trail of alpha particles due to reactions in the detectors is evident for $E_1 \approx 12$ MeV, and the groupings along this trail correspond to inelastic alpha-particle groups observed with a thin Si target. Except for these misplaced particles, the separation between the ^{3}He and alpha-particle bands is excellent. Counters 1 and 2 were 0.5 and 1.5 mm thick, respectively.

ground uncertainties were important, and the estimated error was larger.

A $(\Delta E, E)$ counter telescope composed of silicon surface-barrier detectors was used in conjunction with a 20 000-channel, two-parameter analyzer to separate alpha and ^{3}He particles. The first counter, in a transmission mount, was operated with sufficient bias to deplete the entire thickness of silicon. The total thickness of the two counters was 2 mm; hydrogen isotopes deposited at most 26 MeV and were not analyzed. About half the data were taken with the ΔE and E counters 0.5 and 1.5 mm thick, respectively. The other half were obtained with two counters each 1.0 mm thick. Each of these sets gave excellent separation of the alpha and ^{3}He particles of interest.

The availability of a two-parameter analyzer greatly simplified the separation of particles. The ΔE pulse was digitized by the Y-axis analog-to-digital converter (ADC) operating in its 50-channel mode. The sum of the pulses from both counters was digitized by the ADC for the X axis in its 400-channel mode. Biased amplifiers were used to eliminate small pulses and to make better use of the analyzer memory. Analyzer dead time was determined by counting the same detector pulses with two scalers, one of which registered counts only when the analyzer was busy.

Some difficulty was experienced due to reactions in the detectors, principally inelastic scattering by Si.

TABLE I. Isotopic abundances and thicknesses of targets.

Target	Abundances [atom%]					Thickness (mg/cm²)
	^{90}Zr	^{91}Zr	^{92}Zr	^{94}Zr	^{96}Zr	
^{90}Zr	98.6	0.8	0.4	0.2	~0.05	6.25
^{91}Zr	6.97	89.0	5.23	0.79	0.2	2.85
^{92}Zr	2.45	2.18	93.22	1.97	0.18	7.03

FIG. 2. Previously determined energy levels of Zr isotopes. Only levels to be discussed here are included. Several ^{92}Zr levels not shown here were studied in the ^{91}Zr(α,^{3}He) reaction.

About $\frac{3}{4}\%$ of the elastic alphas appeared with the correct value of ΔE, but at lower values of E than the main peak. This is shown in Fig. 1. Since the ^{3}He particles of interest have almost the same ΔE as the elastic alpha particles, the misplaced pulses can be confused with ^{3}He. The problem was severe for weak ^{3}He groups forward of 30°, but beyond this angle even the weakest ^{3}He group of interest was 10 times as intense as the background of misplaced alpha particles.

The over-all resolution was 200–250 keV. The targets, normally about 350 keV thick, were tilted at the appropriate angle to minimize the spread due to energy loss in the target. Energy straggling in the target was estimated to be about 100 keV. Kinematic broadening varied from 10 to 80 keV over the range of angles studied; this was not a significant contributor to the over-all spread. Tests were made with a target less than 50 keV thick, with narrow slits on the analyzing magnet, and at very low counting rates in an effort to improve the resolution. No improvement was observed, indicating that most of the spread was due to the detectors, in spite

of the fact that 30-keV resolution could be obtained for ^{241}Am alpha particles. A permanent magnet placed in front of the detector to deflect low-energy particles from the target gave no improvement. In view of the limited resolution, most of the data were taken with the object and image slits open quite wide (0.150 in.), corresponding to a calculated acceptance of 130 keV.

The Faraday cup was located about 36 in. from the target. An electrostatic guard ring at the entrance of the cup was used to prevent electrons from entering and leaving. The voltage used on the ring for this experiment was -34 V. However, the collection efficiency did not change when the voltage was varied from -34 to $+100$ V. The collection of charge was also unaffected by putting a $+150$-V bias with respect to ground on the Faraday cup itself. The beam-current integrator was calibrated to an accuracy of 1% by use of a standard ^{241}Am source of known intensity.[13]

The beam direction was determined by taking data on each side of the beam. Because of the rapid variation
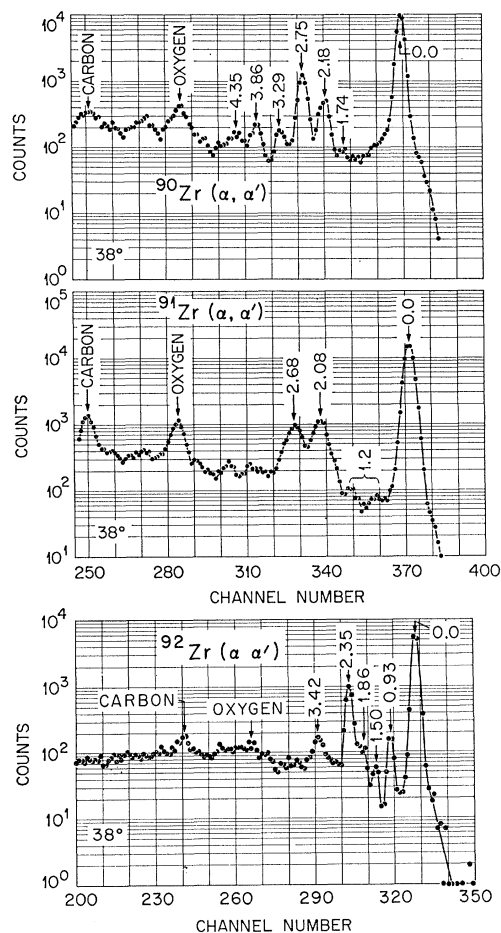
FIG. 3. Alpha-particle spectra at 38° lab from Zr isotopes bombarded with 65-MeV alpha particles. The excitation energies for the prominent peaks are given.

---

[13] R. S. Bender (private communication).
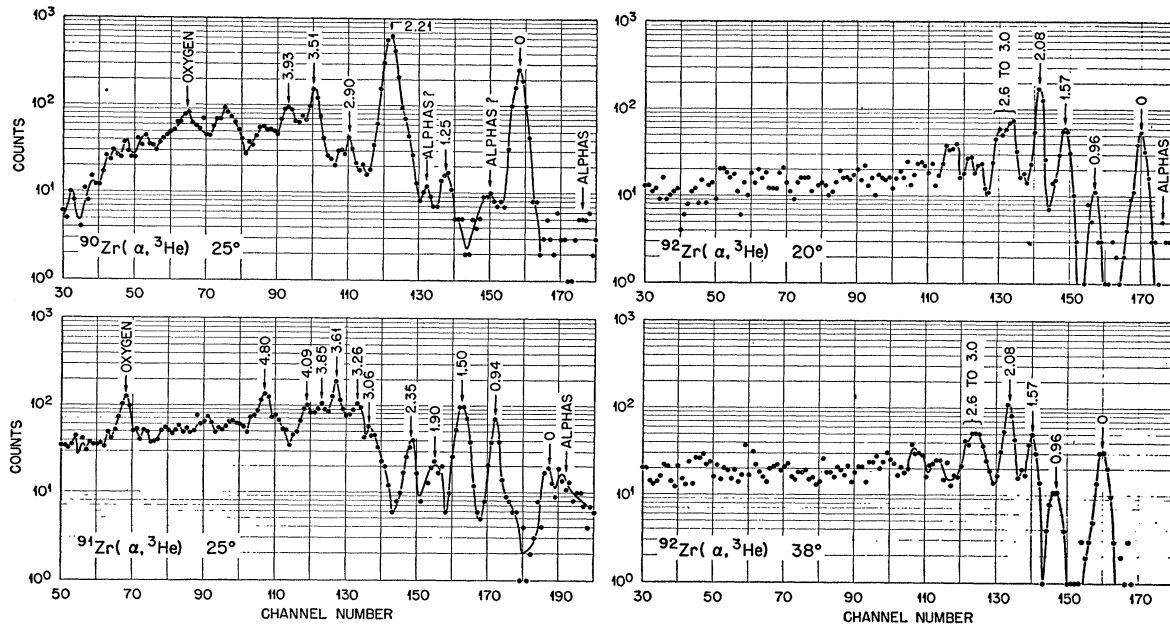
FIG. 4. ³He spectra from Zr isotopes bombarded with 65-MeV alpha particles. The excitation energies for the prominent peaks are given.

with angle of the scattering cross sections, the direction could be measured to within 0.05°. However, errors of as much as 0.4° may exist for small sections of data due to possible shifts in the beam direction after extended cyclotron-off periods.

The beam energy was held fixed by keeping a constant current in the beam analyzing magnet. Care was taken to center the object and image slits of the analyzing magnet on the same line during each scheduling period. The beam energy was found to be 65.0±0.3 MeV. This calculation is based on the 72-in. radius of curvature and the previously measured magnetization curve.[14] This value was confirmed to within 1 MeV by kinematic checks which compared scattering from deuterium and carbon as a function of angle.

After data were accumulated at each angle, the contents of the analyzer memory were dumped on a magnetic tape, which was subsequently processed by an IBM 7090 computer. The number of counts in each channel was listed in a 50×400 matrix. With the same program, alpha-particle and ³He spectra were extracted and plotted semilogarithmically by the printer. The counts in each peak were then added by hand. Another program computed the cross sections and converted quantities to the center-of-mass system.

III. EXPERIMENTAL RESULTS

A. Energy Spectra

A number of energy levels and spins assigned in previous work will be discussed in the following pages. Diagrams showing the levels to be discussed are given

in Fig. 2. The diagrams are not complete; they show only the levels which are of interest here. The ⁹⁰Zr levels were taken from Ref. 15 and the ⁹²Zr levels were primarily taken from Ref. 16. The remainder of the levels were taken from Ref. 9.

Alpha-particle spectra at 38° are shown in Fig. 3. The energy scale for the ⁹²Zr spectrum was determined by assigning an energy of 2.35 MeV to the well-known 3⁻ state. The 2.75 MeV 3⁻ level of ⁹⁰Zr was used to determine the energy scale for the ⁹⁰Zr and ⁹¹Zr spectra. Excitation energies are shown for the prominent peaks.

Helium-3 spectra at 25° from ⁹⁰Zr and ⁹¹Zr and at 20° and 35° from ⁹²Zr are shown in Fig. 4. The excitation energies for the peaks observed are shown in the figure. A small background is apparent, due to elastically scattered alpha particles misplaced from the elastic peak by reactions in the counter (see Fig. 1). The problem is serious only in the region from 10° to 30°.

B. Angular Distributions

Elastic scattering angular distributions are shown in Fig. 5. The ratios of the measured cross sections to the Rutherford cross sections are shown by the dots, the curves being optical-model least-squares fits which will be discussed in Sec. IVA. The shifts in phase and magnitude of the angular distributions at large angles are partly due to the $A^{1/3}$ dependence of the radius, although this does not completely account for them. These differences lead to a slight variation of the optical-model parameters with isotope, as will be shown later.

[14] E. D. Hudson and R. S. Lord (private communication).

[15] S. Bjornholm, O. B. Nielsen, and R. K. Sheline, Phys. Rev. 115, 1613 (1959).

[16] M. E. Bunker, B. J. Dropesky, J. D. Knight, and J. W. Starner, Phys. Rev. 127, 844 (1962).
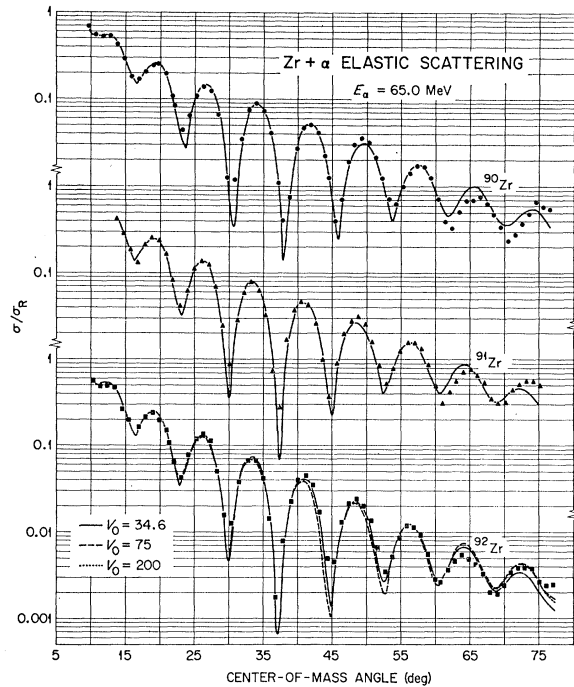
FIG. 5. Ratio of elastic scattering cross sections to the Rutherford cross section. The curves are optical-model least-squares fits. Fits with several potentials are illustrated for ^{92}Zr. The curves for $V_0 = 75$ and $V_0 = 200$ MeV are the same below 65°.

Inelastic scattering angular distributions are shown in Figs. 6, 7, and 8. The smooth curves are distorted-wave predictions discussed in Sec. IVB.1. The angular distributions for all 2$^+$ and 3$^-$ levels are in agreement with the Blair phase rule.[17] The 1.75-MeV group of ^{90}Zr was weakly excited and the points shown are not as reliable as the rest of the data.

The angular distributions for some of the inelastic groups include unresolved levels. The 2.18-MeV group of ^{90}Zr may include a significant contribution from the 5$^-$ level at 2.32 MeV even though the center of the peak remained close to 2.18 MeV in all the spectra. In ^{92}Zr,
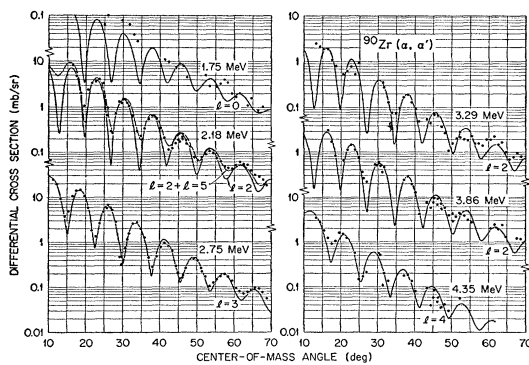
FIG. 6. Differential cross sections for inelastic scattering from ^{90}Zr. The smooth curves are distorted-wave predictions.

[17] J. S. Blair, Phys. Rev. **115**, 928 (1959).

the 0$^+$ level at 1.38 MeV and 4$^+$ level at 1.50 MeV could not be resolved. If this 0$^+$ level is excited as strongly as the 0$^+$ level of ^{90}Zr at 1.75 MeV, it could make no more than a 20% contribution here. In ^{91}Zr, three groups of unresolved states are shown—that labeled 2.08 MeV may include the levels at 1.89, 2.06, 2.21, and 2.35 MeV, while the 2.68-MeV group includes the levels at 2.58 and 2.88 MeV. The 1.2-MeV peak contains several weak groups, corresponding to excitations of 0.9, 1.2, and 1.4 MeV.

At small angles the elastic peak is enormous and its relatively small low-energy tail is comparable with the inelastic intensities, particularly for low-lying states. The forward cross sections for these transitions are less reliable than the large angle data.

The experimental $(\alpha, ^3\text{He})$ angular distributions are shown by the dots in Figs. 9, 10, and 11, along with distorted-wave predictions to be discussed in Sec. IVC. The alpha-particle background at small angles is apparent in a few of the angular distributions. There is a notable lack of structure in these angular distributions as compared with the scattering data.

IV. THEORETICAL INTERPRETATION

The elastic scattering was analyzed in terms of the optical model. Parameters which gave least-squares fits to the elastic scattering were used to generate the distorted waves for inelastic scattering and stripping calculations.
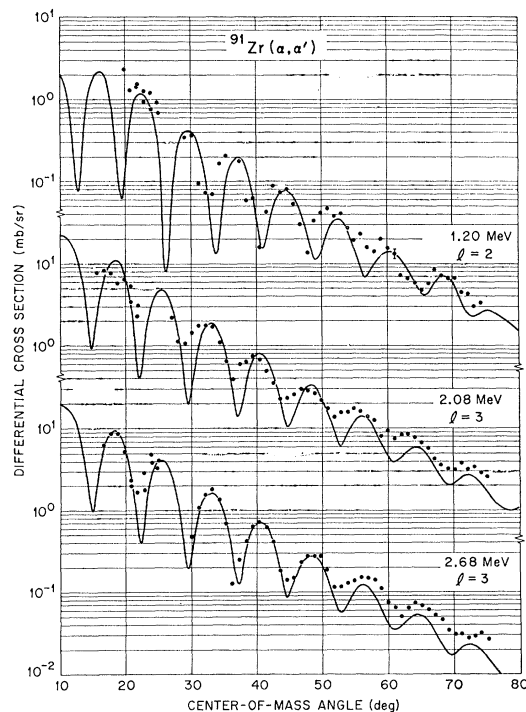
FIG. 7. Differential cross sections for inelastic scattering from ^{91}Zr. The smooth curves are distorted-wave predictions. Each of these angular distributions represents a group of states.
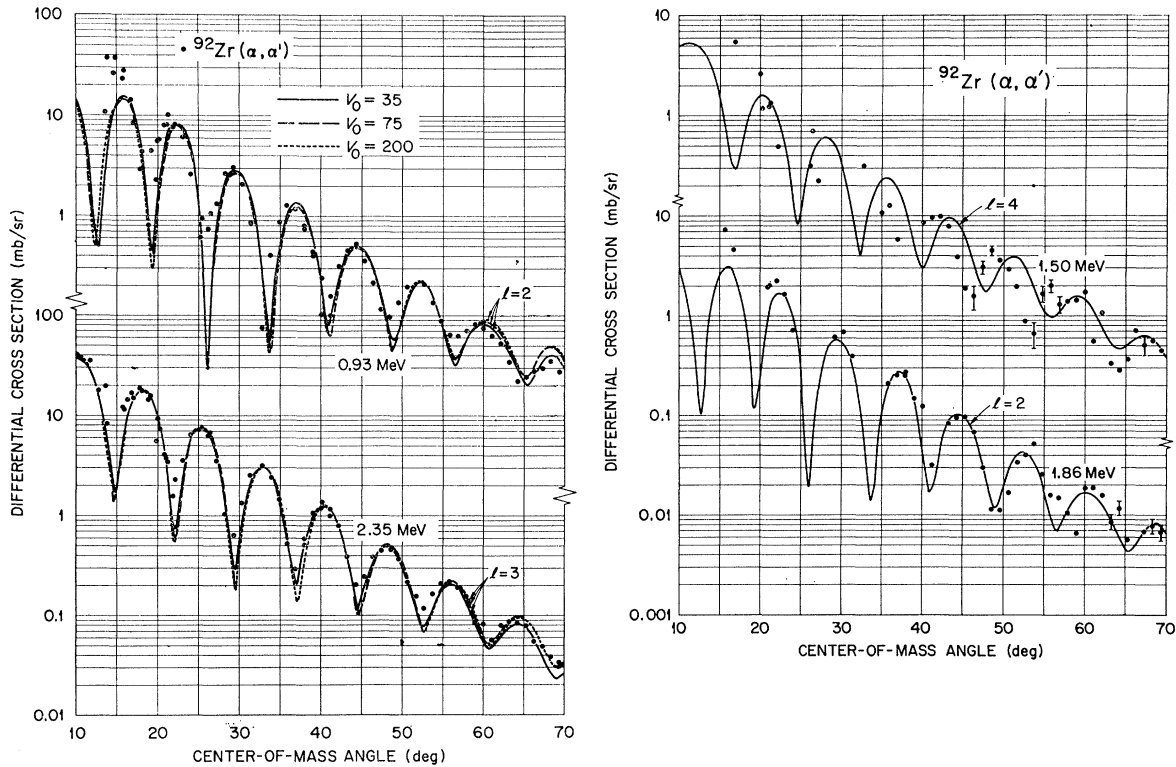
FIG. 8. Differential cross sections for inelastic scattering from ^{92}Zr. The smooth curves are distorted-wave predictions.

FIG. 9. Differential cross sections for ^{90}Zr(α,^{3}He). For the weakly excited groups the cross sections at small angles are probably too large because of contamination from the elastic peak, as indicated by the elastic-scattering curve. The other curves are distorted-wave predictions.
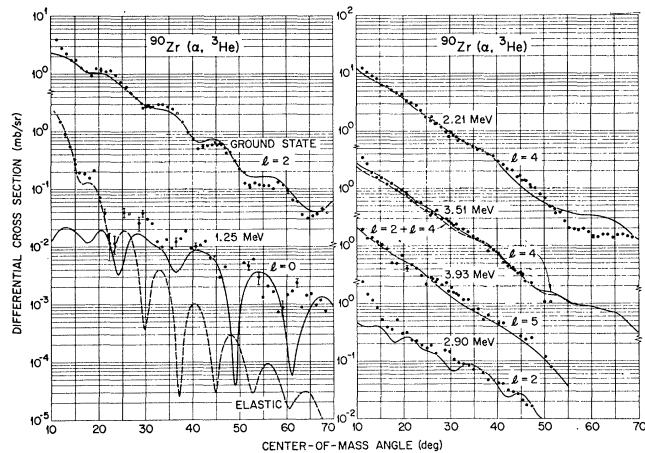
The distorted-wave transition amplitude for the reaction $A(a,b)B$ has the form[18]

$$T = \int d\mathbf{r}_{aA} \int d\mathbf{r}_{bB} \varphi_{bB}^{(-)*}(\mathbf{k}_b,\mathbf{r}_{bB})$$
$$\times \langle b,B | V | a,A \rangle \varphi_{aA}^{(+)}(\mathbf{k}_a,\mathbf{r}_{aA}), \quad (1)$$

where $\mathbf{r}_{iI}$ is the vector distance from particle i to nucleus I. $\varphi_{aA}^{(+)}$ and $\varphi_{bB}^{(-)}$ are the distorted waves for the entrance and exit channels. The expression $\langle b,B | V | a,A \rangle$

[18] R. H. Bassel, R. M. Drisko, and G. R. Satchler, ORNL-3240, 1962 (unpublished).

is the matrix element of the interaction responsible for the transition, taken between the internal states of the initial and final systems. This factor contains the nuclear structure information to be found from the reaction. The zero-range theory is used here, in which the dependence of this factor on $\mathbf{r}_{bB}$ is taken as $\delta[\mathbf{r}_{bB} - (M_A/M_B)\mathbf{r}_{aA}]$. This reduces the double-vector integration in (1) to a single-vector integration. Only reactions with a single l transfer are considered. For this case the matrix element separates into a form factor which gives the radial dependence $F_{lsj}(\mathbf{r})$ and a co-
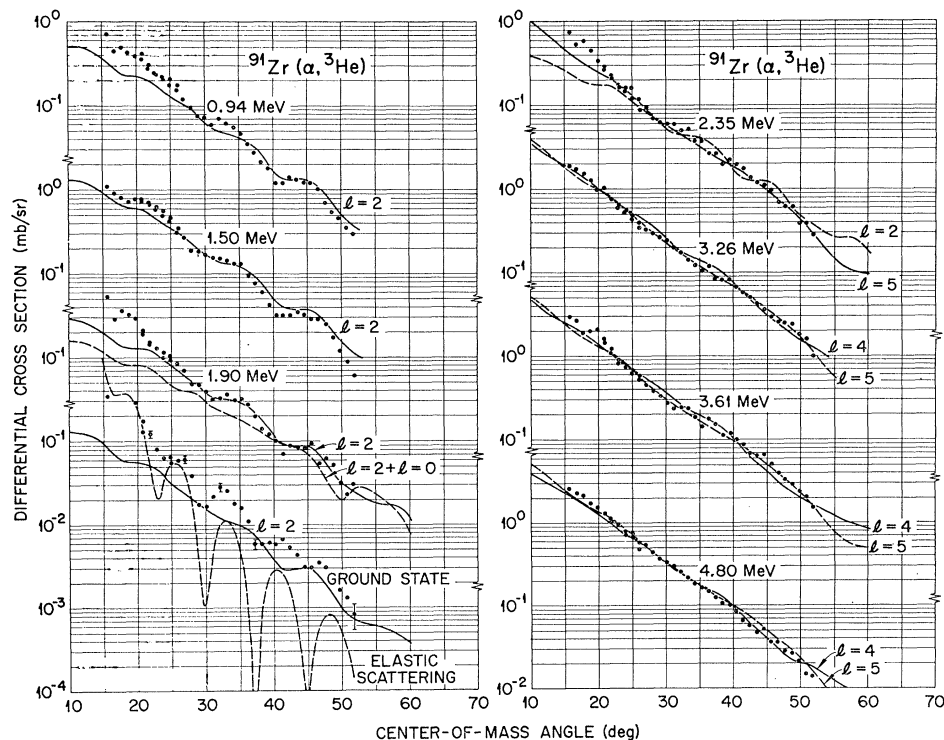
FIG. 10. Differential cross sections for ^{91}Zr$(\alpha,^3$He$)$. For the weakly excited groups the cross sections at small angles are probably too large because of contamination from elastic peak, as indicated by the elastic-scattering curve. The other curves are distorted-wave predictions.

efficient A_{lsj} which includes the strength of the interaction and the square root of the spectroscopic factor.
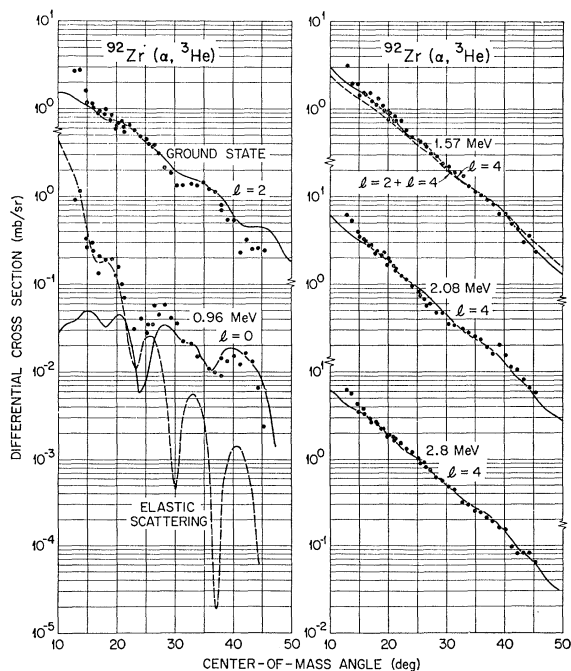
FIG. 11. Differential cross sections for ^{92}Zr$(\alpha,^3$He$)$. For the weakly excited groups the cross sections at small angles are probably too large because of contamination from the elastic peak, as indicated by the elastic-scattering curve. The other curves are distorted-wave predictions.

A. Elastic Scattering

1. Optical-Model Searches

The elastic scattering was analyzed in terms of the potential

$$V(r) = -\frac{V_0}{1+e^x} - \frac{iW_0}{1+e^{x'}} + V_c, \qquad (2)$$

where $x = (r - r_0 A^{1/3})/a$, $x' = (r - r_0' A^{1/3})/a'$, and V_c is the Coulomb potential for a uniformly charged sphere of radius $1.4\, A^{1/3}$ F. For most of the results the added restriction $x = x'$ was invoked, so that only four free parameters V_0, W_0, r_0, and a remained. This restriction entailed only a slight sacrifice in the quality of the fit.

To obtain the best fit with the experimental data, the free parameters were adjusted by an automatic search program[19] to minimize the quantity

$$\chi^2 = \sum_{i=1}^{n}\left(\frac{\sigma_{\mathrm{th}}^{(i)} - \sigma_{\mathrm{expt}}^{(i)}}{\Delta\sigma_{\mathrm{expt}}^{(i)}}\right)^2,$$

where $\sigma_{\mathrm{th}}^{(i)}$ is the calculated differential cross section at angle θ_i, $\sigma_{\mathrm{expt}}^{(i)}$ is the corresponding experimental value, and $\Delta\sigma_{\mathrm{expt}}^{(i)}$ is a weighting factor related to the estimated accuracy of $\sigma_{\mathrm{expt}}^{(i)}$. The absolute value of χ^2 depends heavily on the weighting factors assumed, but comparisons of χ^2 obtained with different parameters using the same experimental data and weights are significant. Graphic comparisons of optical-model predictions and experiment were made to ensure that the

---

[19] The HUNTER program, written by R. M. Drisko.

FIG. 12. Interrelationship of ambiguous optical-model parameters and χ^2 for each set. The experimental data used were the 11°–69° elastic cross sections for ^{92}Zr. These points were obtained from searches in which V_0 was held fixed and W_0, r_0, and a were permitted to vary.
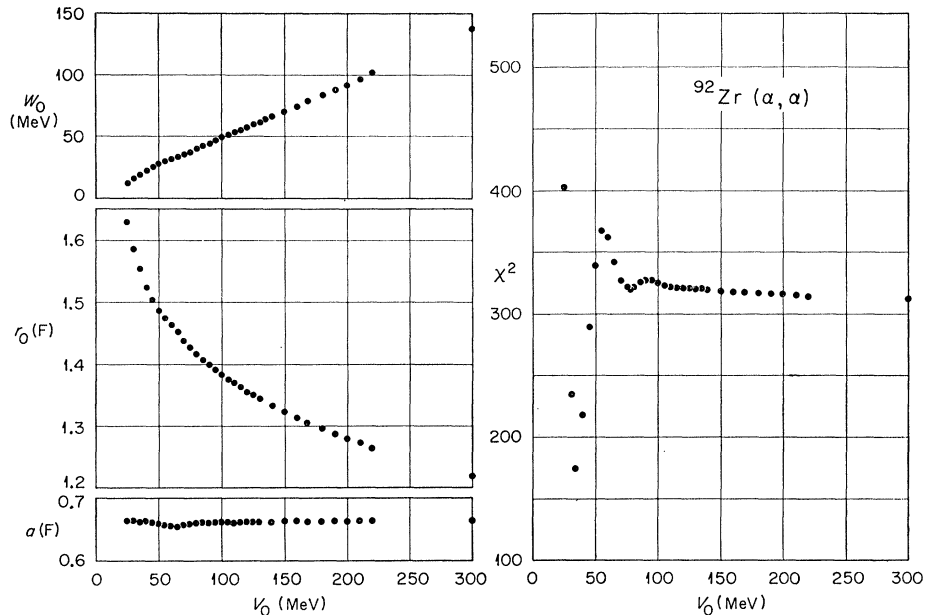
search was not unduly influenced by a few experimental points. The weighting factors $\Delta\sigma_{\text{expt}}^{(i)}$ were chosen to be 5 to 10% of $\sigma_{\text{expt}}^{(i)}$ for points near the maxima in the angular distributions. Values of $\Delta\sigma_{\text{expt}}^{(i)}$ up to 50% of $\sigma_{\text{expt}}^{(i)}$ were chosen for points in the minima because the one-degree aperture on the counter may have affected the depth of the minima significantly. In all cases $\Delta\sigma_{\text{expt}}^{(i)}$ was larger than the standard deviation due to counting statistics.

The potentials giving the minimum values of χ^2 for the full range of data with ^{90}Zr, ^{91}Zr, and ^{92}Zr are listed in the first three lines of Table II, together with χ^2/n, where n is the number of data points. The corresponding fit to the data are shown in Fig. 4 by the solid lines. Also included for comparison is a six-parameter fit for ^{92}Zr. The next two ^{92}Zr potentials listed with larger V_0 gave the fits shown in Fig. 4 by the dashed lines. An earlier four-parameter fit not including the data from 70° to 77° is given in the last line of Table II.

The parameters listed in Table II are somewhat different from those obtained at 43 MeV,[8] namely $V_0=50$ MeV, $W_0=20$ MeV, $r_0=1.52$ F, and $a=0.56$ F. A few searches on ^{92}Zr were made using starting parameters

TABLE II. Parameters giving optimum least-squares fits to the elastic scattering.

Isotope	V_0 (MeV)	W_0 (MeV)	r_0 (F)	a (F)	r_0' (F)	a' (F)	χ^2/n
^{90}Zr	34.63	17.35	1.553	0.631			3.26
^{91}Zr	36.92	19.15	1.550	0.661			5.31
^{92}Zr	34.36	18.92	1.554	0.662			3.34
^{92}Zr	37.18	15.84	1.532	0.664	1.579	0.705	3.12
^{92}Zr	75.00	39.34	1.426	0.661			5.35
^{92}Zr	200.00	97.68	1.277	0.665			5.25
^{92}Zr(11–69°)	34.55	18.86	1.555	0.661			2.41

similar to these. During the initial stages of the search, the values of χ^2 were more than 20 times larger than for the optimum potential, and at large angles the fit was poor. The searches quickly converged to the 35-MeV potential of Table II. With r_0 and a held to the values found at 43 MeV, convergence was obtained with $V_0=43.4$ MeV and $W_0=26.3$ MeV, but χ^2 was then three times as large as when all parameters were allowed to vary.

2. Parameter Ambiguities

Two types of ambiguities in optical model parameters obtained from scattering of complex particles have previously been discussed.[20] Discrete ambiguities were explained as arising from the critical matching of the external wave function to the internal wave function reflected from the angular momentum barrier, and as such show the dependence of the scattering on the optical model in the interior. In addition to the discrete ambiguities, continuous ambiguities arise because changes of one parameter can be compensated for by changes in other parameters.

Three different fits to the ^{92}Zr elastic scattering angular distribution are shown in Fig. 5, labeled by the real depth, V_0. A systematic study showed that the potential with $V_0=34.6$ MeV corresponds to a discrete minimum of χ^2 in parameter space. For $V_0\geq75$ MeV a continuous ambiguity appears which extends to high V_0 values, and hence, over large variations in r_0, V_0, and W_0. This is shown in Fig. 12, a plot of results produced by performing parameter searches on W_0, r_0, and a while holding V_0 fixed. On the left side of Fig. 12 the best-fit

[20] R. M. Drisko, G. R. Satchler, and R. H. Bassel, Phys. Letters **5**, 347 (1963).
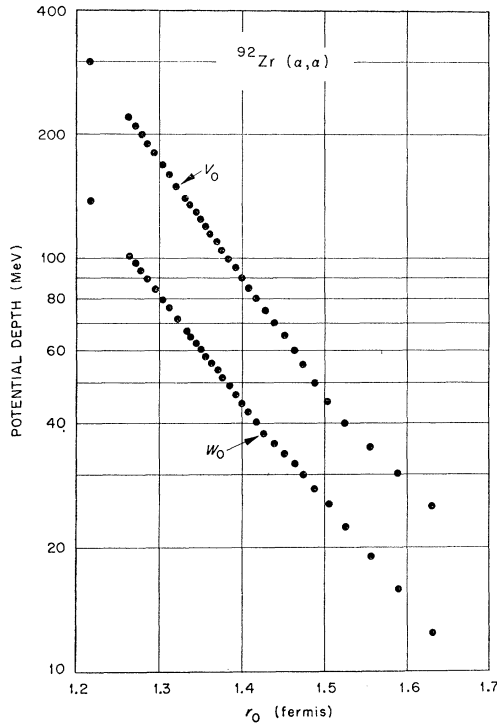
FIG. 13. Dependence of V_0 and W_0 on r_0.

parameters are shown for many values of V_0, while the value of χ^2 for each of these fits is shown on the right. It should be mentioned that at the time these searches were carried out, the elastic scattering had been measured only as far as 69° c.m. A later extension of the data to 77° gave optimum fits (third, fifth, and sixth lines of Table II) with somewhat larger values of χ^2, but the differences in the optimum potential between the original and the extended data were extremely small, as shown in the third and seventh lines of Table I.

To determine if other valleys in parameter space exist, searches were preformed using sets of starting parameters which were different from those shown in Fig. 12. No other acceptable set of parameters was found. For example, a starting point was selected with $V_0 = 200$ MeV, $r_0 = 1.45$ F, $a = 0.5$ F, and $W_0 = 70$ MeV. V_0 and r_0 were held fixed in the first part of the search so that the local minimum could be found. The convergence of this part of the search resulted in $\chi^2 = 15\ 620$. Then letting all the parameters vary, the search quickly converged to the region above $V_0 = 100$ MeV shown in Fig. 12, where χ^2 is about 320.

In a few of the early searches with the ^{92}Zr data, the minima of the angular distribution were weighted in the same way as the neighboring points. The values of χ^2 were generally somewhat larger than those of Fig. 12, and it was noted that other shallow dips in χ^2 similar to the one at $V_0 = 75$ MeV then appeared at higher V_0. More accurate data, especially in the minima, would be needed to determine if these shallow dips are physically significant.

An explanation of the continuous ambiguity follows from the strong absorption of high-energy alpha particles by the nuclear surface. Figure 12 shows that W_0 becomes quite large as V_0 increases, which means that the absorption is strong. Since the particles do not penetrate to the interior, the potential inside the nucleus makes little difference to the elastic scattering. All that is required is that the potentials be equivalent at large radii, as proposed by Igo[21] and discussed in Ref. 20. At large radii the Woods-Saxon potential becomes

$$- (V_0 + iW_0)e^{r_0 A^{1/3}/a}e^{-r/a}.$$

This asymptotic form is the same for all sets of parameters satisfying the conditions

$$a = \text{constant},$$
$$\ln V_0 \propto r_0,$$

and

$$\ln W_0 \propto r_0.$$

Figure 12 shows that the first condition is satisfied. The other two conditions hold for the solutions with large V_0, as shown in Fig. 13.

The transition from the discrete to the continuous ambiguity can be clarified by a comparison of the radial wave functions for the 35-MeV potential and for one of the deeper wells. The magnitude of the wave function for a number of partial waves for potentials with $V_0 = 35$ and $V_0 = 200$ MeV are shown in Fig. 14. For the shallow potential the wave functions at small separation distances are finite and oscillatory which indicates the importance of reflections from the angular-momentum barrier in the interior. For the deep potential the wave functions are attenuated and only the potential at the surface plays a role in the scattering. The similarity at large radii is necessary since both potentials give much the same scattering.

3. Comparisons among ^{90}Zr, ^{91}Zr, and ^{92}Zr

According to the adiabatic approximation,[17] elastic scattering angular distributions for strongly absorbed particles depend on $kR_0\theta$, where k is the relative momentum, R_0 is the nuclear radius, $r_0 A^{1/3}$, and θ is the scattering angle. The optical model gives approximately the same dependence. The shifts in phase seen in the experimental data of Fig. 5 do not follow this dependence precisely. The small differences which occur require slightly different parameters in the optical model, as shown in Table II. For ^{90}Zr and ^{91}Zr fewer searches were made and the long continuous ambiguity was not investigated in detail. The parameters found for these nuclei are shown by the points in Fig. 15. For comparison, the results for ^{92}Zr from Fig. 12 are reproduced here by the solid lines. The most notable feature of these results is that ^{90}Zr seems to have a less diffuse surface than the other two isotopes. Although small changes in

[21] G. Igo, Phys. Rev. Letters 1, 72 (1958); Phys. Rev. 115, 1665 (1959).
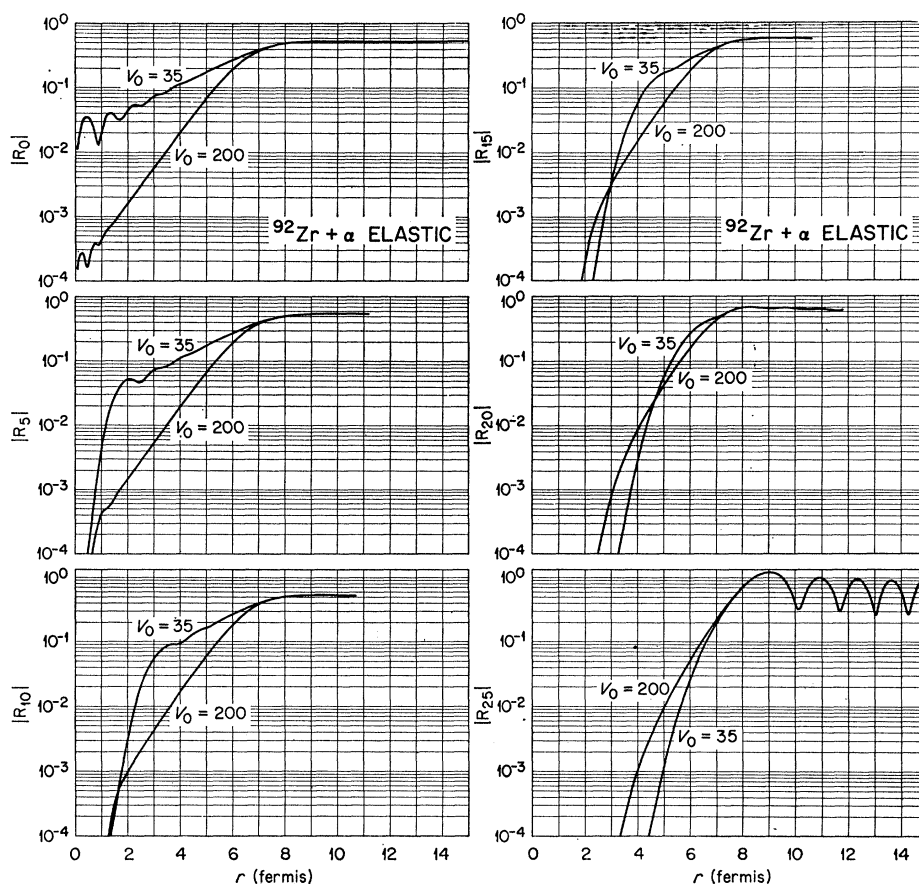
FIG. 14. Magnitudes of selected radial wave functions for the 35- and 200-MeV potentials.

the normalization and other experimentally determined quantities can cause shifts in the optical-model parameters of the order of the differences found here, these differences are believed to be qualitatively significant.

B. Inelastic Scattering

For inelastic scattering one need only assume that the interaction in (1) is local and neglect exchange terms to satisfy the zero-range assumption. The zero spin of the alpha particles greatly simplifies the results for the transition amplitude.

The distorted-wave program JULIE[22] was used to compute the angular distributions. These were subsequently normalized to fit the experimental data by adjusting a parameter in the theory. Collective-model predictions were obtained for all the states observed. A few shell-model calculations assuming single configurations in both the initial and final states were performed for comparison.

1. Collective Model

The collective model uses a nonspherical optical potential. The spherical part produces the elastic scattering and the nonspherical part is identified with the inter-

[22] Program written by R. M. Drisko.

action responsible for the inelastic scattering. Only one-phonon excitations are considered here. The form factor is then dependent upon the radial derivative of the optical-model potential.[1] The deformation parameter β_l is the only adjustable parameter in the calculation; it is determined by normalization of the calculation to the experimental data.

Most of the calculations were performed assuming that only the real part of the Woods-Saxon potential is deformed. The four-parameter potentials with $V_0 \sim 35$ MeV (Table II) were used for both the entrance and exit channels. Coulomb excitation was included for all transitions with $l < 4$. A few trial calculations for the strong 2^+ and 3^- levels of ^{92}Zr were made with four-parameter potentials of other real depths, and with a complex interaction for deformations of both the real and imaginary parts of the 6-parameter potential; details are given in the next section.

(a) ^{92}Zr(α,α'). Distorted-wave predictions assuming real interactions are compared with inelastic scattering angular distributions from ^{92}Zr in Fig. 8. The normalizations to the data are specified by the values of β_l given in Table III. Predictions are shown for the strong 2^+ level at 0.93 MeV and the 3^- level at 2.35 MeV with three different optical potentials (Table II), each designated by its V_0. It is clear that the inelastic scatter-
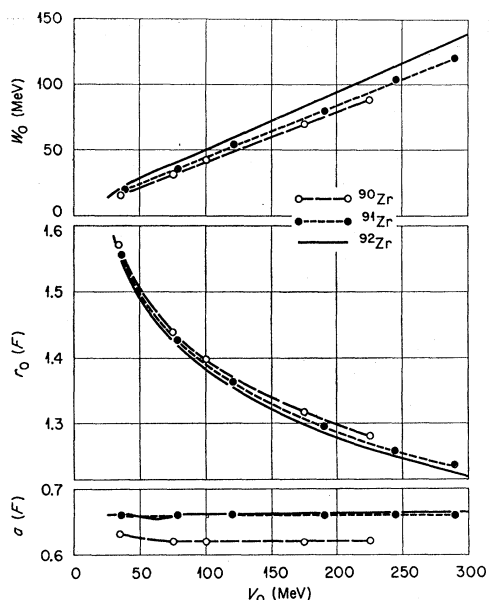
FIG. 15. Comparison of optical-model parameters for ^{90}Zr, ^{91}Zr, and ^{92}Zr. Fits to the experimental data were obtained with parameters given by the points.

ing data do not enable one to distinguish among the ambiguous potentials. The deformation parameter for a given state differs by 15% for the three fits, but the deformation length $\beta_l R_0$ differs by only 5%. The importance of $\beta_l R_0$ has been discussed previously.[23] The β_2 agrees with the value found for the combined 2$^+$ levels of ^{92}Zr and ^{94}Zr by Coulomb excitation of natural zirconium.[24]

Complex coupling was investigated for these two levels using the 6-parameter potential of Table II. The fit of the angular distributions was qualitatively no better than when real interactions were used, so that this additional complication was not included in the remainder of the calculations. On the other hand, the values of β_l were significantly different, about 13% smaller (see Table III). Including the complex interaction in the four-parameter model consists of scaling β_l by $1/(1+W_0^2/V_0^2)^{1/2}$, which, from examination of Table II, yields β_l values reduced by some 12% from those found from the real interaction. A similar effect was found for proton inelastic scattering.[4] These β_l values are somewhat smaller than those found from deuteron scattering analyzed with a complex interaction,[25] but the $\beta_l R_0$ values are in good agreement with the $\beta_l R_0'$ values extracted from the deuteron analysis. This result suggests that the imaginary amplitude is

[23] J. S. Blair, in *Proceedings of the Conference on Direct Interactions and Nuclear Reaction Mechanisms*, edited by E. Clementel and C. Villi (Gordon and Breach, Science Publishers, Inc., New York, 1963), pp. 669–694.
[24] P. H. Stelson and F. K. McGowan, Phys. Rev. **110**, 489 (1958).
[25] R. K. Jolly, Phys. Rev. **139**, B318 (1965).

TABLE III. Deformation parameters for states of ^{92}Zr.

Excitation (MeV)	l	V_0 (MeV)	β_l This experiment	β_l Other sources	$\beta_l R_0$
0.93	2	34.5	0.106	0.100[a]	0.74
0.93	2	75.7	0.111		0.72
0.93	2	200.0	0.123		0.71
0.93	2	37.2[c]	0.092	0.10[b]	
2.35	3	34.5	0.151		1.06
2.35	3	75.7	0.162		1.04
2.35	3	200.0	0.174		1.00
2.35	3	37.2[c]	0.132	0.14[b]	
1.50	(4)	34.5	0.054		0.38
1.86	2	34.5	0.048		0.34

[a] Coulomb excitation (Ref. 24).
[b] (d,d') at 15 MeV (Ref. 25).
[c] Complex interaction and six-parameter optical potential used.

dominant for deuteron inelastic scattering, in agreement with the findings of Dickens, Perey, and Satchler.[26]

The angular distribution predicted for the 2$^+$ level at 1.86 MeV agrees well with the data, but the 4$^+$ state at 1.50 MeV is out of phase by about $\frac{1}{4}$ of an oscillation. The 0$^+$ level at 1.38 MeV, which is not resolved from the 4$^+$ level here, is not expected to contribute much to the cross section, as explained earlier (Sec. IIIB).

Jolly[25] found that for 15-MeV deuterons the 2$^+$ level at 1.86 MeV and this 4$^+$ have similar angular distributions, and he concluded that they, together with 0$^+$ at 1.38 MeV, might be members of a two-phonon triplet. In the present case, the phase of the 2$^+$ level at 1.86 MeV is different from the 4$^+$. However, phase shifts between states of a triplet can occur if they have different ratios of multiple excitations to direct excitations.

To analyze two-phonon states, coupled-channel calculations[27] are ordinarily used. Tamura[28] carried out some exploratory calculations for the ^{92}Zr data presented here, assuming that the 2$^+$ level at 1.86 MeV and the 4$^+$ level at 1.50 MeV were strongly coupled to the one-phonon 2$^+$ level at 0.93 MeV. The phase of the 4$^+$ prediction agreed well with the data, but the agreement was not as good for the 1.86-MeV state. These calculations were not pursued because it was felt that single-particle effects may be more important than collective effects for these levels.

(b) ^{90}Zr(α,α'). Distorted-wave predictions for the ^{90}Zr inelastic scattering angular distributions are shown in Fig. 6. The predicted angular distributions for the strong 2$^+$ and 3$^-$ levels at 2.18 and 2.75 MeV are in satisfactory agreement with the data. The influence of the unresolved 5$^-$ state at 2.32 MeV is shown by the dashed curve. This is a sum of the $l=2$ curve (solid line) reduced by 30% and an $l=5$ prediction using $\beta_5 = 0.056$, obtained from alpha scattering at 34 MeV.[29] Good agree-

[26] J. K. Dickens, F. G. Perey, and G. R. Satchler, Nucl. Phys. **73**, 529 (1965).
[27] T. Tamura, Rev. Mod. Phys. **37**, 679 (1965).
[28] T. Tamura (private communication).
[29] H. Ogata, S. Tomita, M. Inoue, Y. Okuma, and I. Kumabe, Phys. Letters **17**, 280 (1965).

TABLE IV. Deformation parameters for states of ^{90}Zr.

Excitation (MeV)	l	V_0 (MeV)	β_l This experiment	β_l Other sources	$\beta_l R_0$ (F) This experiment	$\beta_l R_0$ (F) Other sources
1.75	0	34.6	~0.0083		~0.058	
2.18[a]	2	34.6	0.058	0.073,[b] 0.09[c]	0.403	0.512,[b] 0.484
2.75	3	34.6	0.120	0.12,[b] 0.19[c]	0.836	0.842,[b] 1.02[c]
3.29	2	34.6	0.035		0.245	
3.86	2	34.6	0.043		0.300	
4.35	4	34.6	0.048		0.331	

[a] Corrected for $\beta_5 = 0.056$ contribution.
[b] (α,α') at 34 MeV (Ref. 29).
[c] (p,p') at 19 MeV (Ref. 4).

ment of $l=2$ predictions with the data for the 3.29-MeV peak and the 3.86-MeV peak supports a spin assignment of 2^+ to these states. The good fit of the $l=4$ prediction with the 4.35-MeV angular distribution supports a spin assignment of 4^+, although some doubt exists because of the poor agreement of theory and data for the known 4^+ level of ^{92}Zr. These assignments agree with the spin assignment of 2 to the 3.86-MeV level and doubtful spin assignments of (0,2) and (4) to the 3.29- and 4.35-MeV levels found by inelastic proton scattering.[4]

The values of β_l are given in Table IV. For the 2.75-MeV level, β_3 agrees well with the result from scattering of 34-MeV alpha particles. However, β_2 for the 2.18-MeV level (corrected for the 5^- state) is 27% smaller. This may indicate that the collective model is a poorer description of the 2^+ excitation than of the 3^-. If the 5^- contribution is not subtracted (solid curve in Fig. 6) then $\beta_2 = 0.066$ and $\beta_2 R_0 = 0.456$. The (p,p') results given in the table are those obtained with a real interaction. With a complex interaction the (p,p') experiment gives values of $\beta_2 = 0.07$ and $\beta_3 = 0.16$. Dividing the β_l obtained here by 1.13, the ratio of real to complex interactions found in ^{92}Zr, one would expect the β_2 and β_3 in ^{90}Zr obtained with complex interactions to be about 0.051 and 0.106. With these numbers the deformation lengths found from the two experiments agree, on average, within 15%.

(c) ^{91}Zr(α,α'). The ^{91}Zr(α,α') angular distributions shown in Fig. 7 are for groups of unresolved states, so that precise spectroscopic information cannot be obtained. If the two groups at 2.08 and 2.68 MeV arise primarily from coupling of the last neutron to the ^{90}Zr core excited to the 3^- state at 2.75 MeV, the sum of the cross sections for these two groups should be the same as the cross section for the excitation of the 3^- state of ^{90}Zr. Experimentally the sum is about 1.5 times larger, which may indicate that other types of states contribute significantly to the unresolved groups. The $l=3$ distorted-wave prediction fits the angular distribution for the 2.68-MeV group better than the 2.08-MeV group; the maxima of the latter appear at angles about one degree less than for the 2.68-MeV group. Strong single-particle states in the region around 2.2 MeV have been observed in $(\alpha,^3\text{He})$ results to be presented later. Excitation of these may add to or mix with the

collective vibration, thereby accounting for the difference in behavior of the data and the $l=3$ collective model prediction. It is also possible that a significant portion of the $l=2$ strength based on the first 2^+ level of ^{90}Zr is included, as suggested below. Because of these complications these data neither support nor conflict with the core-excitation model.

The entire region of the spectra between the elastic scattering peak and the peak at 2.08 MeV seemed to be out of phase with the elastic scattering with the possible exception of a peak at 1.4 MeV. Other peaks were observed at 0.9 and 1.2 MeV. The former is probably due to the ^{92}Zr and ^{94}Zr impurity in the target, and accounts for about 40% of the out-of-phase cross section. The angular distribution for this entire region is labeled 1.2 MeV in Fig. 7. The maxima are at the same angles as an $l=2$ distorted-wave prediction. If these $l=2$ states arise from the coupling of the additional neutron to the first 2^+ state of ^{90}Zr, the cross section of this group should equal the cross section for exciting that 2^+ level. However, the 1.2-MeV cross section corrected for impurities is only about 15% as large, indicating either that most of the $l=2$ collective oscillation lies higher, perhaps in the 2.08-MeV group, or else that the core-excitation model does not describe these states.

2. Shell Model

The single-particle interpretation of inelastic scattering has been described in some detail.[30] The interaction causing the nuclear transition is taken to be the sum of interactions between the incident alpha particle and the nucleons in the target nucleus

$$V(\mathbf{r}, \mathbf{s}_\alpha, \xi) = \sum_i v_{i\alpha}((\mathbf{r} - \mathbf{r}_i), \mathbf{s}_\alpha, \mathbf{s}_i),$$

where ξ represents the internal coordinates of the target, $\mathbf{r}$ and $\mathbf{r}_i$ are the positions of the alpha particle and ith target nucleon, and $\mathbf{s}_\alpha$ and $\mathbf{s}_i$ are their spins. To be completely rigorous, nucleon-nucleon interactions should be used and an additional sum taken over the nucleons of the alpha particle. In this case spin-dependent parts would remain in the interaction. However, the assumption is made here that these parts vanish when the sum over the alpha-particle nucleons is carried out since $s_\alpha = 0$. The alpha-particle nucleon interaction then becomes

$$v_{i\alpha} = -V_\alpha g(|\mathbf{r} - \mathbf{r}_i|),$$

where the separation into a strength and a factor to give the spatial dependence is for convenience. At the present time the form of g is not well known. A phenomenological approach has been adopted, with the intention of finding a suitable interaction. Since only exploratory calculations have been made thus far, they have been limited to pure configurations.

Two forms of the interaction g were used, the Gaussian

---

[30] G. R. Satchler, Nucl. Phys. **77**, 481 (1966).
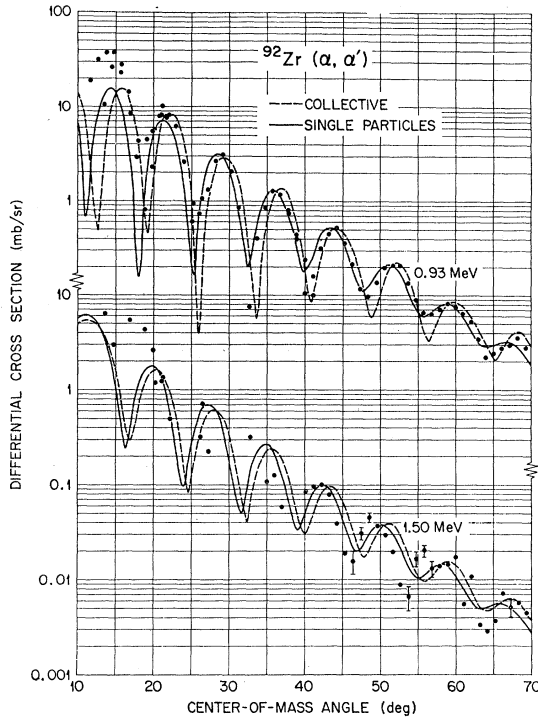
FIG. 16. Comparison of distorted-wave predictions for single-particle and collective excitations of the first 2^+(0.93 MeV) and 4^+ (1.50 MeV) levels of ^{92}Zr.

of range R

$$g(|\mathbf{r}-\mathbf{r}_i|)=e^{-|\mathbf{r}-\mathbf{r}_i|^2/R^2},$$

and the Yukawa interaction

$$g(|\mathbf{r}-\mathbf{r}_i|)=\frac{1}{\alpha|\mathbf{r}-\mathbf{r}_i|}e^{-\alpha|\mathbf{r}-\mathbf{r}_i|},$$

with range parameter α.

The calculation considered here was based on the assumption that the levels of ^{92}Zr at 0, 0.93, and 1.50 MeV are due to $(d_{5/2})^2$ neutron configurations coupled to spins of 0, 2, and 4, respectively. The form factors were computed using the code ATHENA[31] under the following conditions. The radial wave functions were those for a neutron in a Woods-Saxon potential with $r_0=1.2$ F and $a=0.7$ F, and with a spin-orbit term equal to 25 times the Thomas term. The depth was adjusted to give the binding energy of the neutron in the ground state of ^{91}Zr. Since only neutron excitations were considered here, a Coulomb potential was not needed. The wave functions for an equivalent nonlocal potential were obtained in the local-energy approximation[32] using a range $\beta=0.85$ F, and were normalized to unity over all space.

These form factors were then used in the program JULIE[22] to obtain the distorted-wave predictions for the inelastic scattering cross sections. The optical-model

---

[31] Program written by M. B. Johnson and L. W. Owen.
[32] F. G. Perey and A. M. Saruis, Nucl. Phys. **70**, 225 (1965).

parameters with $V_0=34.36$ MeV (Table II) were used for both the entrance- and exit-channel distorted waves. The resulting predictions were then compared with the experimental data for the 0.93 (2^+) and 1.50 MeV (4^+) levels of ^{92}Zr, with the strength parameter V_α adjusted for the best fit to each curve. For a consistent picture, one requires the same value of V_α for the two transitions.

The angular-distribution predictions for the Gaussian interaction with $R=2.0$ F are shown in Fig. 16, in comparison with the collective model predictions and the experimental data. The single-particle predictions are generally better than the collective predictions, but the required values of V_α are in strong disagreement—73.8 MeV for the 2^+ level and 39.4 MeV for the 4^+. The inconsistency could be reduced by assuming a range of 2.5 F. The strength was then 34.5 MeV for the 2^+ level and 22.3 MeV for the 4^+ level. In this case the predicted angular distributions were shifted about one degree toward smaller angles making the prediction for the 4^+ angular distribution very good, but the prediction for the 2^+ angular distribution was then very poor.

Using the Yukawa interaction with $\alpha=0.5$ $(F)^{-1}$, the agreement of the 4^+ prediction with the data is good, but there is a shift of about 1.5 deg between the 2^+ data and prediction. The values of V_α were in better agreement in this case, namely 41.4 MeV for the 2^+ and 33.9 MeV for the 4^+. Although neither form of the interaction is completely satisfactory, on the whole the Yukawa interaction is superior. The Yukawa interaction also gave a better fit to inelastic scattering of protons from ^{90}Zr.[4]

The configurations assumed here were, of course, oversimplified. Experimentally, the 2^+ excitation is stronger than the simple calculations indicate. More complicated configurations may contribute to the 2^+ state, thereby making it appear more collective. To obtain accurate information on the alpha-particle nucleon interaction, one would need scattering from states for which the wave functions are well known.

C. Stripping Reactions

1. Method of Calculation

The results presented here are restricted to zero range. The relevant theory has been presented elsewhere.[18] The transition is assumed to be due to the interaction of the ^{3}He nucleus with the transferred neutron. The interaction is taken to be central. The form factor is the radial bound-state wave function of the stripped neutron, which is taken as the solution of Schrödinger's equation for a Woods-Saxon potential with $r_0=1.2$ F, $a=0.7$ F, and a depth adjusted to give an eigenvalue equal to the binding energy of the transferred neutron. Spin-orbit coupling and nonlocal effects were considered in a few trial calculations described in Sec. C.7.

With these assumptions, a reduced cross section $\sigma(\theta)$ is calculated by means of the distorted-wave program

TABLE V. Exit-channel parameters used in distorted-wave calculations for $(\alpha,{}^3\text{He})$ reactions.

V_0 (MeV)	W_0 (MeV)	r_0 (F)	a (F)	r_0' (F)	a' (F)	r_c (F)	Comment
178.0	25.7	1.14	0.723	1.544	0.800	1.4	a
142.9	12.97	1.082	0.795	1.659	0.757	1.4	b
177.2	20.4	1.12	0.743	1.583	0.780	1.4	b, c

[a] Parameters which fit elastic scattering of 22.0-MeV ^{3}He from ^{62}Ni (Ref. 34).
[b] Parameters which fit elastic scattering of 43.6-MeV ^{3}He from ^{90}Zr with W_0 increased from 16.4 to 20.4 MeV in the 177.2-MeV set (Ref. 36).
[c] Parameters used to determine spectroscopic factors in conjunction with 100-MeV alpha potentials which fit elastic scattering (Fig. 15).

JULIE.[22] Assuming pure configurations, the distorted-waves cross section is then calculated from[18]

$$\left(\frac{d\sigma}{d\Omega}\right)_{\text{DW}} = \frac{2J_B+1}{2J_A+1}\frac{N}{2s+1}S\sigma(\theta),$$

where J_A and J_B are the spins of the target and residual nuclei, respectively, and s is the spin of the transferred particle. The factor N accounts for the overlap of the alpha particle and the n-^{3}He system as well as the strength of the interaction, and S is the spectroscopic factor. A rough estimate of $N=6.53$ was obtained by using the asymptotic form of the n-^{3}He wave function obtained from the solution of Schrödinger's equation with a binding energy equal to that of the neutron in the alpha particle.

In view of the drastic simplifications made in these calculations, it was expected that an additional normalization factor R would be necessary to achieve agreement with the measured cross sections:

$$(d\sigma/d\Omega)_{\text{exp}} = R(d\sigma/d\Omega)_{\text{DW}}.$$

The approach taken here was to adjust R empirically at the start of the analysis by comparison with other data, and thereafter keep it constant. This is described below in Sec. 3. A similar procedure was used by Alford, Blau, and Cline.[33]

2. Effect of Optical Parameters and Radial Cutoff

Although the exit-channel ^{3}He energy was about 50 MeV, the only potential available when the first calculations were made was one obtained from data on the scattering of 22 MeV ^{3}He by ^{62}Ni.[34] This potential had the form of (2) with the parameters given in the first line of Table V, and was used to obtain the curves in Fig. 17. In the bottom part of Fig. 17 the $l=2$ predictions for three different entrance-channel potentials specified by V_0 (with the other parameters given by Fig. 15) are compared with the data leading to the $2d_{5/2}$ ground state of ^{91}Zr. It is clear that the curves are sensitive to the choice of entrance-channel optical parameters. The prediction for $V_0=83$ MeV matches the data

[33] W. P. Alford, L. M. Blau, and D. Cline, Nucl. Phys. **61**, 368 (1965).
[34] D. D. Armstrong and A. G. Blair (private communication).
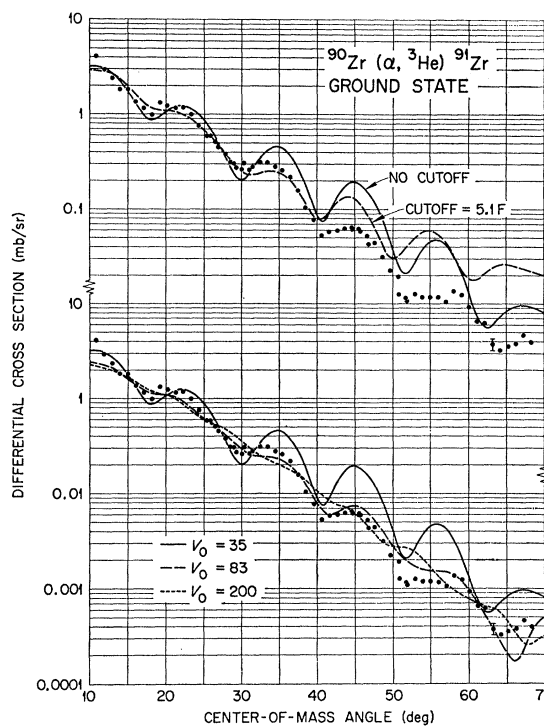
FIG. 17. Dependence of distorted-wave prediction on radial cutoff and on entrance-channel optical parameters.

best; the one for $V_0=35$ MeV is much less satisfactory. The magnitude of the latter is about 25% greater than the other two, but in this figure the normalizations were adjusted freely for the best fit.

A lower cutoff on the radial integral was introduced in an effort to improve the 35-MeV fit, since finite-range effects tend to decrease the part of the transition amplitude coming from the nuclear interior.[35] The curves in the top part of Fig. 17 compare the same data with $V_0=35$-MeV predictions for $l=2$, with and without a radial cutoff. The effect is small and the improvement is largely confined to the 30°–40° region. Other choices of cutoff radius gave slightly different predictions; the one shown was the most successful. The magnitude of the prediction with a 5.1-F cutoff is 15% smaller than without a cutoff but again the normalization in this figure was adjusted for the best fit to the angular distribution. For the $2d_{5/2}$ ground state of ^{93}Zr the effect of the radial cutoff and the fit with the data were very much the same. For the group at 2.21 MeV in ^{91}Zr, an $l=4$ prediction was made with the same parameters. Here the effect of the cutoff was smaller and the agreement with the data was not improved. With the exception of the one curve at the top of Fig. 17, none of the distorted-wave predictions shown in this paper include a radial cutoff. The $l=2$ predictions with the 83-MeV and 200-MeV potentials are insensitive to the cutoff radius, as might have been anticipated from the small

[35] R. M. Drisko and G. W. Satchler, Phys. Letters **9**, 342 (1964)
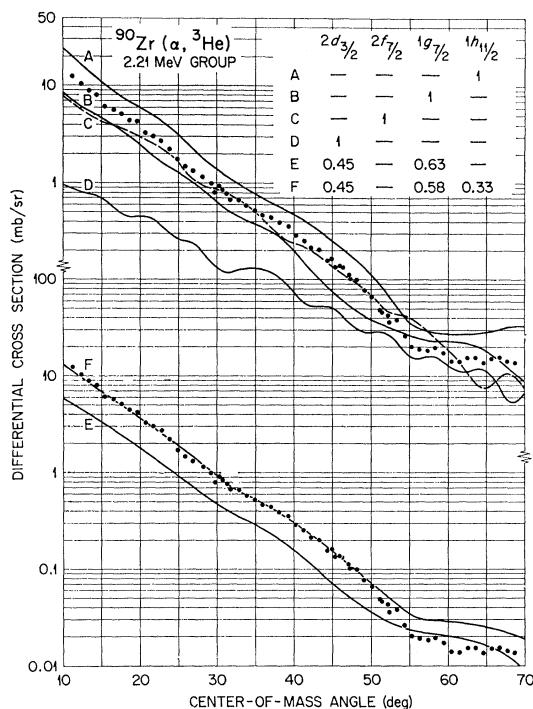
FIG. 18. Distorted-wave predictions for ^{90}Zr(α,^{3}He) to the group at 2.21 MeV. The spectroscopic factors for the various curves are given in the table.

values of the radial wave function inside the nucleus (Fig. 14).

The choice of exit-channel parameters influenced the selection of the best-fitting entrance-channel optical-model parameters. During the course of this work, parameters became available for Woods-Saxon potentials which fit the elastic scattering of 43.6-MeV ^{3}He particles from ^{90}Zr.[36] Two good fits were found, one with $V_0=142.9$ MeV and the other with $V_0=177.2$ MeV. Some (α,^{3}He) calculations were done with each potential. The best fit to the data for stripping to the ground state of ^{91}Zr using the 142.9-MeV potential was obtained with the alpha scattering potential with $V_0=75$ MeV. Using the 177.2-MeV ^{3}He potential, the best fit was obtained with the alpha potential having $V_0=100$ MeV. The remaining discussion will be restricted to this latter set of parameters. The exit-channel parameters are given in Table V (third line); the entrance-channel parameters may be read from the curves in Fig. 15 for the appropriate target nucleus. It should be mentioned that W_0 for the exit channel was increased from 16.4 to 20.4 MeV, since W_0 is expected to be larger for the higher energy ($\sim$50 MeV) of the ^{3}He particles here. The effect of increasing W_0 is to make the angular distribution a little steeper, reduce the oscillatory structure, and decrease the magnitude by about thirty percent. This difference in normalization was con-

[36] E. F. Gibson, J. J. Kraushaar, B. W. Ridley, and M. E. Rickey (private communication).

sistent for all the states studied, so the relative spectroscopic factors do not depend on this choice.

3. Determination of R

Spectroscopic factors for the states of interest here have previously been obtained by Cohen and Chubinsky with (d,p) reactions.[9] The ground states of ^{91}Zr and ^{93}Zr have spin assignments of $\frac{5}{2}^{+}$. By using the Cohen-Chubinsky spectroscopic factor of 0.89 for the ^{91}Zr ground state, R was found to be 15.76, while it was 19.83 with their value of $S=0.54$ for the ^{93}Zr ground state. In all the results to be presented, the average of these numbers, $R=17.80$, was used. Recalling that $(d\sigma/d\Omega)_{\text{calc}}$ depends partially on the optical potential and cutoff radius, the agreement with the value of 16.7 obtained from the ^{16}O(^{3}He,α) reaction at low bombarding energies is quite good.[33] A recent re-analysis of the same data by Cline, Alford, and Blau[37] using a different entrance-channel potential gave $R\approx24$, which may still be considered to be in satisfactory agreement with the present results.

4. ^{90}Zr(α,^{3}He)^{91}Zr Reaction

The angular distributions for stripping to various levels of ^{91}Zr are compared with the distorted-wave predictions in Fig. 9. The normalization for the ground-state transition corresponds to $S=0.79$ rather than the Cohen-Chubinsky value of 0.89, since an average R was used as explained above. However, this result is in good agreement with the value of 0.75 obtained in a (d,p) experiment at 12.0-MeV bombardment energy by Dickens, Perey, and Silva.[38] It likewise agrees well with the value of 0.72 obtained from an analysis[39] of the ground-state transition in the reaction ^{91}Zr(p,d)^{90}Zr at 22 MeV.[40]

Although alpha-particle contamination of the data for the $3s_{1/2}$ state at 1.25 MeV was significant at small angles, it should be less than 10% of the cross section beyond 30 deg. The $l=0$ prediction in Fig. 9 was normalized to the data at large angles by choosing $S=0.31$. This is in poor agreement with the value of 0.72 found by Cohen and Chubinsky, but considering the accuracy of the data agrees satisfactorily with the value of 0.41 obtained by Dickens, Perey, and Silva.

A pure $l=4$ prediction ($g_{7/2}$) is shown in Fig. 9 for the 2.21-MeV group. The normalization corresponds to $S=1.44$ which is larger than unity, the total $g_{7/2}$ strength

[37] D. Cline, W. P. Alford, and L. M. Blau, Nucl. Phys. 73, 33 (1965).

[38] J. K. Dickens, F. G. Perey, and R. J. Silva (private communication).

[39] R. H. Bassel, R. M. Drisko, and G. R. Satchler, in *Proceedings of the International Symposium on Direct Interactions and Nuclear Reaction Mechanisms*, edited by E. Clementel and C. Villi (Gordon and Breach, Science Publishers, Inc., New York, 1963), pp. 520–523.

[40] C. D. Goodman, J. B. Ball, and C. B. Fulmer, in *Proceedings of the International Symposium on Direct Interactions and Nuclear Reaction Mechanisms*, edited by E. Clementel and C. Villi (Gordon and Breach, Science Publishers, Inc., New York, 1963), pp. 524–526.

expected for this nucleus. In Fig. 18, distorted-wave predictions for stripping to $d_{3/2}$, $f_{7/2}$, $g_{7/2}$ and $h_{11/2}$ with $S=1.0$ for each are compared with the data. With a shift in normalization corresponding to $S=0.65$, the $h_{11/2}$ curve would fit the data better than the $g_{7/2}$. According to Cohen and Chubinsky, this group consists of a number of unresolved states including the $g_{7/2}$ level to 1.89 MeV, the $d_{3/2}$ level at 2.06 MeV, the strong $g_{7/2}$ level at 2.21 MeV, and the level at 2.35 MeV with a doubtful assignment of $g_{7/2}$. The spectroscopic factor given by Cohen and Chubinsky for the $d_{3/2}$ level is 0.45 and the sum of those for the $g_{7/2}$ levels is 0.63. Curve E of Fig. 18 is the distorted-wave prediction using the Cohen-Chubinsky spectroscopic factors. The curve is too low over most of the angular range. If the normalization were adjusted for a satisfactory fit with the data, the additional $g_{7/2}$ or $d_{3/2}$ strength would exceed the theoretically expected sums of spectroscopic factors. If the peak at 2.35 MeV is assumed to be $h_{11/2}$ with $S=0.33$, curve F is obtained, using the previous values of S for the other levels. The fit to the data is satisfactory over a wider range of angles than would be possible with curve E, even assuming the normalization were increased sufficiently.

The $d_{3/2}$ prediction for the group at 2.90 MeV requires $S=0.60$. Cohen and Chubinsky report $d_{3/2}$ states at 2.88 and 3.11 MeV with a total $S=0.18$ which is in poor agreement with the present result. The spectra were not clear cut in the present case and transitions to levels other than the two reported by Cohen and Chubinsky may be included here.

The group labeled 3.51 MeV in Fig. 9 is composed of the unresolved $g_{7/2}$ group at 3.49 MeV and the $d_{3/2}$ levels at 3.30 and 3.70 MeV, having spectroscopic factors are 0.33, 0.15, and 0.10, respectively, according to Cohen and Chubinsky. Dickens, Perey, and Silva[38] have given $S=0.24$ for the $g_{7/2}$ level and $S\sim0.1$ for each of the two $d_{3/2}$ levels. Calculating the sum of the $d_{3/2}$ contributions with $S=0.25$ and adding to it the $g_{7/2}$ prediction with the strength adjusted for the best fit with the data, we obtain the dashed curve shown. The $g_{7/2}$ strength for this curve is 0.34, in excellent agreement with the Cohen-Chubinsky results. If the $l=2$ contribution is omitted, a $g_{7/2}$ strength of 0.43 is required (solid curve).

The peak at 3.93 MeV contains the two groups observed by Cohen and Chubinsky at 3.89 and 4.12 MeV which were assigned configurations of $f_{7/2}$ and $g_{7/2}$ and $S=0.042$ and 0.056, respectively. The peak observed here is too strong to correspond to these spectroscopic factors. Distorted-wave predictions for $l=4$ and $l=5$ fit the experimental angular distribution almost equally well. If the peak were due to $g_{7/2}$ excitations, the spectroscopic factor would be 0.28. The prediction shown in Fig. 9 is from an $h_{11/2}$ calculation with $S=0.12$.

5. $^{91}Zr(\alpha,^{3}He)^{92}Zr$ Reaction

Although the spins of many of the levels of ^{92}Zr of interest here are well established, several of those

at higher excitation are not. Following Cohen and Chubinsky[9] we express results in terms of S', defined by

$$S'=[(2J_B+1)/(2J_A+1)]S.$$

The levels with uncertain spin are not shown in Fig. 2.

Distorted-wave predictions for stripping to states of ^{92}Zr are compared with the data in Fig. 10. The stripping to the ground state of ^{92}Zr was weak and appeared to be contaminated with alpha particles. Normalization of an $l=2$ prediction to the data at large angles yielded $S'=0.19$ (i.e., $S=1.14$). This may be compared with $S'=0.24$ ($S=1.44$) from the (d,p) reaction,[9] and $S=1$ from analysis[39] of the ground-to-ground (p,d) reaction on ^{92}Zr.[40]

The $l=2$ predictions agree well with the data for the levels at 0.94 and 1.50 MeV with $S'=0.95$ and 2.71. These are close to the values 1.11 and 2.9 obtained from (d,p) results.[9]

The group observed at 1.9 MeV includes the 2^+ levels at 1.86 and 2.05 MeV. According to Cohen and Chubinsky, these states are excited by $l=2$ and $l=0$, respectively, with $S'=0.36$ and 0.30. The prediction for the $(\alpha,^{3}He)$ reaction with these values of S' is shown by the dashed line in Fig. 10. The solid curve shows a pure $l=2$ prediction for $S'=0.70$, which seems to give better agreement with the angular distribution.

Cohen and Chubinsky report an $l=2$ group at 2.40 MeV with $S'=0.23$. An $l=2$ prediction for the group at 2.35 MeV is shown in Fig. 10 with $S'=1.01$, which is far larger than the value given by Cohen and Chubinsky. If this group is due mainly to a transition to the 3^- level of ^{92}Zr at this energy, an odd l value is required. A fit, shown as a solid curve in Fig. 9, can be achieved with an $h_{11/2}$ neutron with $S'=0.47$, which is only 3.9% of the total expected $h_{11/2}$ strength. However, if this group actually consists of transitions to two different levels, and if we adopt the Cohen-Chubinsky value of $S'=0.23$ for the $l=2$ strength, then an adequate fit to the data can be obtained with $S'=0.37$ for $l=5$.

The values of S' used for the $l=4$ fits in Fig. 10 to the groups at 3.26, 3.61, and 4.80 MeV are 3.10, 4.47, and 4.76, respectively. Near 3.26 MeV, Cohen and Chubinsky found only $l=0$ levels. They report $l=2$ states near 3.61 MeV. A pure $l=2$ interpretation of the present data would require $S'=6.88$, which is 8.7 times larger than the sum of the $l=2$ strength they reported. This suggests that these two peaks consist mainly of states which were not observed in the (d,p) experiment and that they probably correspond to either $l=4$ or $l=5$ transfers. The $l=5$ predictions fit well with $S'=1.93$ and 2.68 for the 3.26- and 3.61-MeV groups, respectively. In the (d,p) experiment, an $l=4$ peak was observed at 4.80 MeV and was assigned $S'=2.4$. The peak observed here includes perhaps two $l=2$ levels with a total $S'=0.58$ according to Cohen and Chubinsky, but even allowing for this, the agreement is poor. The $l=5$ prediction fits well with $S'=2.97$.
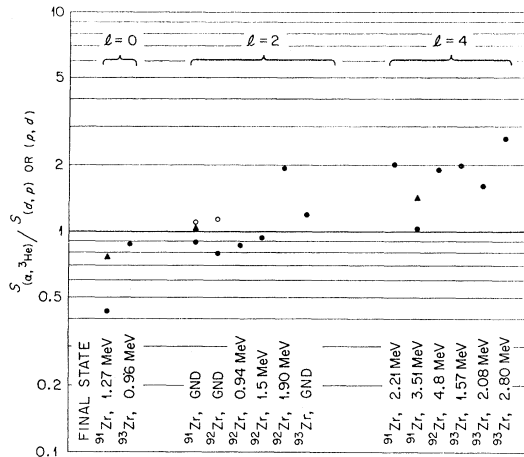
FIG. 19. Comparison of the spectroscopic factors obtained in the present experiment with values previously found: ●(d,p), Ref. 9; ▲(d,p), Ref. 38; ○(p,d), Ref. 39.

The total S' for all $g_{7/2}(l=4)$ transitions should be 8.0. The sum of the S' for all the possible $l=4$ states discussed above already exceeds this value by a factor of 1.64, which may indicate that transitions higher than $l=4$ are important. In this connection it should be pointed out that other states with excitations of 3.0 to 4.5 MeV are strongly excited in the $(\alpha,{}^3\mathrm{He})$ reaction (see Fig. 4). The $l=0$ and 2 strength reported by Cohen and Chubinsky for nearby levels is insufficient to account for the observed yields.

6. $^{92}Zr(\alpha,{}^3He)^{93}Zr$ Reaction

Distorted-wave predictions for stripping to states in ^{93}Zr are given in Fig. 11, together with the experimental data. The ground state is $d_{5/2}$; the normalization corresponds to a spectroscopic factor of 0.64. As before, the difference between this result and the value of 0.54 found by Cohen and Chubinsky arises from the averaging between the ^{91}Zr and ^{93}Zr ground states in fixing R. If the level at 0.28 MeV is excited in this reaction, the spectra show that its intensity is less than 10% of the ground-state intensity.

At small angles the $s_{1/2}$ level at 0.96 MeV was highly contaminated with alpha particles, as shown by the dashed curve. However, the problem is not serious at large angles and normalization there yielded a spectroscopic factor of 0.79. This is in satisfactory agreement with the value of 0.91 obtained by Cohen and Chubinsky.

The peak at 1.57 MeV contains a $d_{3/2}$ level at 1.45 MeV with $S=0.38$ and a level at 1.64 MeV with a doubtful assignment of $g_{7/2}$ and $S=0.11$, as reported by Cohen and Chubinsky. An increase of the $g_{7/2}$ spectroscopic factor from 0.11 to 0.22 improves the agreement with the $(\alpha,{}^3\mathrm{He})$ data. This result is shown as a dashed curve in Fig. 11. A pure $l=4$ curve with $S=0.36$ also gives a good fit, as indicated by the solid curve.

The peak at 2.08 MeV contains three levels reported

by Cohen and Chubinsky: $s_{1/2}$ at 1.94 MeV with $S=0.21$, $g_{7/2}$ at 2.32 MeV with $S=0.09$, and one at 2.08 MeV with a doubtful assignment of $g_{7/2}$ and $S=0.42$. The differential cross section for the level at 0.96 MeV suggests that the $s_{1/2}$ level included here should make a negligible contribution. The curve in Fig. 11 is a $g_{7/2}$ distorted-wave prediction with $S=0.82$. This spectroscopic factor is in poor agreement with 0.51, the sum of the values obtained from the (d,p) reactions to the two g states.

The group at 2.80 MeV in Fig. 3 showed two prominent peaks in most of the spectra. It may contain the $d_{3/2}$ states at 2.50 and 2.78 MeV with spectroscopic factors of 0.24 and 0.21, and the $g_{7/2}$ state at 3.02 MeV with $S=0.30$, as reported by Cohen and Chubinsky. The $l=4$ angular distribution fits the data well. Subtracting the $d_{3/2}$ strength given above, the $g_{7/2}$ strength is found to be 0.79, far bigger than 0.30.

7. Discussion of Results

A comparison of the $(\alpha,{}^3\mathrm{He})$ with the (d,p) and (p,d) spectroscopic factors is shown in Fig. 19. For those peaks which were unresolved in the $(\alpha,{}^3\mathrm{He})$ experiment, theoretical predictions based on the (d,p) spectroscopic factors were used for all but the strongest state. The spectroscopic factor for the strongest state was then derived from fitting the data. The 2.35-MeV group in ^{92}Zr is omitted from the comparison because of the strong possibility of an $l=5$ contribution, making extraction of the $l=2$ strength very uncertain. The 2.9-MeV group is omitted because of the possibility that states other than $l=2$ make substantial contributions.

With the exception of the 1.9-MeV group of ^{92}Zr, the $l=0$ and $l=2$ spectroscopic factors are in reasonable agreement with the (d,p) and (p,d) results. However, all the $l=4$ spectroscopic factors from $(\alpha,{}^3\mathrm{He})$ are larger than those from (d,p), except for the 3.51-MeV state of ^{91}Zr. Since the (d,p) spectroscopic factors are consistent with sum rules,[9] the additional strength seen with $(\alpha,{}^3\mathrm{He})$ may be due to inclusion of transitions with other l values, in particular, $l=5$. The angular distributions for $l=5$ are difficult to distinguish from $l=4$ (see Fig. 18). The apparent absence of $l=5$ transitions in the (d,p) experiments is not surprising since those experiments were done at 15 MeV and could not have been expected to show weak $l=5$ transitions. On the other hand, the almost constant factor by which the $l=4$ spectroscopic factors differ suggests that the distorted-wave calculations may be inadequate.

To explain the difference in the agreement for $l=0$ and 2 and $l=4$, one needs to find a shortcoming of the theory which is spin dependent. The neglect of the spin-orbit coupling of the bound-state neutron quickly comes to mind. Sample calculations were performed in which a spin-orbit potential equal to 25 times the Thomas term for nucleons was included in the solution for the bound-state wave functions. The magnitude of the $d_{5/2}$

prediction was increased by about 6%, that of the $d_{3/2}$ prediction decreased by about 8%, and that of the $g_{7/2}$ decreased about 26%. This effect therefore tends to exaggerate rather than reduce the discrepancy in spectroscopic factors.

The use of nonlocal potentials in the local-energy approximation[41] was also investigated. Inclusion of a non-local potential with a range of 0.85 F for the bound-state wave function results in an increase in the cross section of about 30% and a slightly steeper decrease with angle. The additional inclusion of nonlocal potentials with ranges of 0.2 F in the solution for the distorted waves does not change the normalization but does increase the slope. However, these nonlocal effects were the same for $g_{7/2}$ as for $d_{5/2}$, so they did not explain the discrepancies. Calculations with finite-range interactions are not expected to give significantly different results because the nonlocality tends to reduce the effects of finite range.[42]

It may be recalled that the optical potential for the exit channel was extrapolated from data at a lower energy, and that ambiguities in both channels forced a somewhat arbitrary choice of potentials. Measurement of the ^{3}He elastic scattering at the appropriate energy may help explain the $l=4$ discrepancies, and may limit the choice of acceptable ^{3}He potentials; such experiments are now in progress at this laboratory.

Note added in proof. Optical potentials have now been obtained for ^{3}He+Zr at 51 MeV. Re-analysis of the $(\alpha,^3\text{He})$ transitions to the ground states of ^{91}Zr and ^{93}Zr give $R=15.5$ and 15.6, respectively. This improves the agreement with the (α,p) spectroscopic factors for $l=0$ and $l=2$, but accentuates the disagreement for $l=4$.

V. SUMMARY AND CONCLUSIONS

Optical-model analysis of the elastic scattering from ^{92}Zr yielded a distinct minimum in x^2 at a real well depth of 34.6 MeV. A continuous ambiguity was found for $V_0 \gtrsim 75$ MeV and was followed up to $V_0=300$ MeV; these potentials are the same at large radii. The transition from discrete to continuous ambiguity as V_0 increases can be traced to the accompanying increase in the absorptive part of the potential. Data for ^{90}Zr and ^{91}Zr isotopes required a slight change of optical

potentials for the best fits. The ^{90}Zr surface seems to be somewhat less diffuse than the other two.

Collective-model calculations for the inelastic scattering showed no preference among the ambiguous potentials. The collective-model distorted-wave predictions were generally in good agreement with the data. The values of $\beta_l R_0$ were consistent with the results of other experiments.

Shell-model calculations yielded inelastic angular distributions in fair agreement with the data for the 2$^+$ and 4$^+$ levels of ^{92}Zr at 0.93 and 1.50 MeV, respectively. These were treated as $(d_{5/2})^2$ configurations with a phenomenological Gaussian or Yukawa interaction. Although there was a slight preference for the Yukawa interaction, neither of the interactions was completely satisfactory.

The $(\alpha,^3\text{He})$ angular distributions did show sensitivity to the choice of optical-model parameters. Selecting among the potentials for the entrance and exit channels which describe the elastic scattering well, a combinaiton was found which predicted angular distributions in good agreement with the data. Adjusting the normalization by an empirical factor of 17.80 to compensate for certain rough approximations made in applying the distorted-wave calculations, satisfactory agreement with with spectroscopic factors from (d,p) and (p,d) reactions was obtained for $l=0$ and $l=2$ transitions. The $l=4$ spectroscopic factors were generally larger for $(\alpha,^3\text{He})$. The discrepancy could not be resolved by consideration of spin-orbit or nonlocal effects; it may be due to the presence of transitions with $l>4$, to incorrect selection of the optical potentials, or to some other unknown failure of the theory.

[41] F. G. Perey and B. Buck, Nucl. Phys. **32**, 353 (1962); F. G. Perey and D. S. Saxon, Phys. Letters **10**, 107 (1964).
[42] J. K. Dickens, R. M. Drisko, F. G. Perey, and G. R. Satchler, Phys. Letters **15**, 337 (1965).

FIG. 1. Photograph of analyzer display. All channels containing at least one count are shown by a bright spot. The trail of alpha particles due to reactions in the detectors is evident for $E_1 \approx 12$ MeV, and the groupings along this trail correspond to inelastic alpha-particle groups observed with a thin Si target. Except for these misplaced particles, the separation between the ³He and alpha-particle bands is excellent. Counters 1 and 2 were 0.5 and 1.5 mm thick, respectively.